

On the Geometry of the High-Velocity Ejecta of the Peculiar Type Ia Supernova 2000cx

R. C. Thomas¹, David Branch¹, E. Baron¹, Ken’ichi Nomoto², Weidong Li³, and Alexei V. Filippenko³

ABSTRACT

High-velocity features in Type Ia supernova spectra provide a way to probe the outer layers of these explosions. The maximum-light spectra of the unique Type Ia supernova 2000cx exhibit interesting Ca II features with high-velocity components. The infrared triplet absorption is quadruply notched, while the H&K absorption is wide and flat. Stimulated by a three-dimensional interpretation of similar Ca II features in another Type Ia supernova (SN 2001el, Kasen et al. 2003), we present alternative spherically symmetric and three-dimensional ejecta models to fit the high-velocity ($v > 16000 \text{ km s}^{-1}$) Ca II features of SN 2000cx. We also present simple estimates of the high-velocity ejecta mass for a few trial compositions and discuss their implications for explosion modelling.

Subject headings: supernovae: individual (SN 2000cx) — radiative transfer

1. Introduction

One-dimensional (1D) white dwarf explosion models like W7 (Nomoto et al. 1984) have been used to synthesize spectra in good agreement with those observed in Type Ia supernovae (SNe Ia). But recent polarization observations of the SNe Ia 1999by (Howell et al. 2001) and 2001el (Kasen et al. 2003) indicate that at least some SN Ia envelopes deviate from spherical symmetry.

The strongest case for such deviation appears in the Ca II lines of SN 2001el. This event exhibits an unusual Ca II infrared (IR) triplet in its flux spectrum about a week

¹Department of Physics and Astronomy, Nielsen Hall RM 131, Norman, OK 73019
(thomas,branch,baron)@mail.nhn.ou.edu

²Department of Astronomy & Research Center for the Early Universe, University of Tokyo, Bunkyo-ku, Tokyo, 113-0033, Japan

³Department of Astronomy, 601 Campbell Hall, University of California, Berkeley, CA 94720-3411

before maximum brightness. Two triplets are evident: one corresponds to photospheric-velocity (PV) material and the other to higher-velocity (HV) material. In the polarization spectrum, the HV feature coincides with significant intrinsic net polarization. Kasen et al. (2003) investigate a number of envelope models to account for the HV feature. Generally, they conclude that (1) incomplete covering of the photosphere and (2) some deviation from spherical symmetry are required to produce the HV features. Unfortunately, conditions did not permit simultaneous observation of the blue spectrum so a corresponding phenomenon in the Ca II H&K feature remains unconfirmed.

Another unusual Ca II feature is found in the spectrum of the peculiar SN 2000cx (Li et al. 2001). Near maximum light, its ostensible Ca II IR triplet possesses an interesting quadruply notched feature perhaps due to what Li et al. call “some unique distribution of Ca in the ejecta of SN 2000cx,” extending to high velocity. The wavelength coverage of the near-maximum light spectra is excellent. Though polarization data in the same wavelengths are not available, simultaneous fits of the H&K and IR triplet features may help constrain at least the HV photospheric covering fraction (if indeed the HV material is not distributed in spherical symmetry).

It remains unclear why clumpy HV ejecta could occur in SNe Ia. Detailed synthetic spectropolarimetry has yet to test explosion models free from the constraint of spherical symmetry (Khokhlov 2000; Hillebrandt et al. 2000; Gamezo et al. 2003). These explosion calculations have neither proceeded to the free-expansion phase nor provided abundance distributions required for detailed spectrum synthesis. On the other hand, methods for calculating synthetic spectra from three-dimensional (3D) models of SNe are in their infancy (Thomas et al. 2002; Kasen et al. 2003). Hence parameterized, direct analysis of observed SN spectra remains a powerful way of guiding explosion modellers to replicate geometrical phenomena in their models.

Here we apply such direct methods to SN 2000cx to suggest geometrical constraints on its HV ejecta. We concern ourselves mainly with the Ca II features at a single epoch; a comprehensive direct analysis of the spectra is forthcoming (D. Branch et al., in preparation). In §2 of this paper we present the spectra and identify the features of interest. In §3 we use the 1D direct analysis code **Synow** and the analogous 3D code **Brute** to test a few geometrical distributions of Ca II line optical depth. We discuss the candidate models and estimate the HV ejecta mass in §4, using a variety of possible compositions. Conclusions appear in §5.

2. Spectra

In Figure 1 are three spectra of SN 2000cx collected near maximum light, originally presented by Li et al. (2001). The usual SN Ia absorptions from Si II (near 6150 Å) and S II (near 5400 Å) are accompanied by unusual absorptions due to Fe III (near 4300 Å and 5000 Å). There is very little, if any, signature of Fe II.

Between 7900 Å and 8400 Å are a series of four notches. Usually at this phase, only absorption from the two stronger lines of the triplet ($\lambda\lambda 8542, 8662$ — often blended) are visible in this region, and these are the best candidates for the two redder notches. The two bluer ones are perfectly consistent with a Ca II IR triplet shifted to about 22000 km s⁻¹ toward the observer. The bluest and weakest line of the Ca II IR triplet ($\lambda 8498$) is approximately ten times weaker than $\lambda 8542$, and is likely heavily blended by that line. Other ions are unlikely to produce the notches; candidates such as O I are unconvincing due to the absence or weakness of concomitant lines in the spectra.

The corresponding Ca II H&K absorption feature (3500 Å to 3800 Å) is wide and flat. A collection of currently unidentified narrow absorption features obliterates its emission peak.

Figure 2 displays the Ca II features of SNe 2000cx and 1994D near maximum light in terms of velocity relative to the observer. The top half of each panel is the H&K feature relative to the *gf*-weighted doublet wavelength (3945 Å), while the bottom half is the IR triplet relative to its *gf*-weighted wavelength (8579 Å). Figures 2a, 2b, and 2c are from SN 2000cx at days 2, 6, and 7 past maximum light, respectively. For comparison, the normal SN Ia 1994D Ca II features at day 3 past maximum appear in Figure 2d.

Hatano et al. (1999a) use HV Ca II and Fe II to improve their synthetic fits of SN 1994D. In that SN, the effect of the HV Ca II is much less pronounced than in SN 2000cx. In fact, the IR triplet of SN 2000cx has a HV absorption that has a depth relative to the continuum between that of SNe 1994D and 2001el.

Note that the four notches in the SN 2000cx IR triplet do not evolve appreciably in velocity space over time. A one-to-one correspondence between the notches in the IR triplet and any depressions in the H&K feature cannot be firmly established by these plots, but the overall velocity ranges of the two features match. We henceforth designate the parts of the Ca II features forming above 16000 km s⁻¹ relative to the *gf*-weighted wavelengths of the H&K and IR triplet as the HV features. Since the three SN 2000cx spectra in Figures 1 and 2 are all very similar, we restrict the focus of the remainder of this paper to the spectrum obtained two days after maximum light.

3. Fits

The simplest conceptual model of a SN Ia between a few days to months after explosion consists of an homologously expanding envelope surrounding a continuum-emitting, optically thick core. The decay of freshly synthesized ^{56}Ni to ^{56}Fe at the center of the SN releases energy in the form of γ -rays. This energy diffuses outward and degrades to ultraviolet, visible, and infrared wavelengths via interactions with the matter in the SN atmosphere.

This elementary model has been implemented in a variety of codes intended for the empirical analysis of SN spectra (Jeffery & Branch 1990; Fisher 2000; Mazzali & Lucy 1993). These codes all implement a sharply defined photosphere at some radius as a lower boundary for a line-forming envelope. They utilize the Sobolev approximation (Sobolev 1947; Castor 1970) to construct radiation field estimates for given optical depth distributions. Optical depths may be parameterized (in velocity space and wavelength) or determined from a selected abundance and density model with or without a self-consistent temperature structure.

These codes have proved useful for fitting observed spectra to constrain the structure of SN envelopes. This empirical process is called “direct” analysis to distinguish it from “detailed” analysis where the full radiative transfer and non-local thermodynamic equilibrium rate equations are solved (Hauschildt & Baron 1999). The results of direct analysis provide useful guidance to detailed spectrum modellers.

Synow is a direct analysis code that has been used to fit many spectra of various types of SNe, e.g., SN Ia 1994D (Hatano et al. 1999a), several SNe Ib (Branch et al. 2002), SN Ic 1994I (Millard et al. 1999), and SN II 1999em (Baron et al. 2000). **Synow** relies on spherical symmetry and parameterized line optical depth. Each selected ion is assigned an optical depth in a “reference” line, usually a strong optical line. All other line optical depths for the same ion are determined assuming local thermodynamic equilibrium (LTE) excitation of the levels at some specified temperature. The optical depths are scaled as a function of radius to fall off exponentially or according to a power law. The full details of **Synow** are available in Fisher (2000).

We have recently developed a code similar to **Synow** in its degree of parameterization, but free from the constraint of spherical symmetry. This code, **Brute**, is based on Monte Carlo techniques presented in a series of papers by Lucy and Mazzali (i.e. Mazzali & Lucy 1993), and will be discussed in detail elsewhere (R. C. Thomas, in preparation). In **Brute**, spatial parameterization of line optical depth is managed through a 3D template. To establish the radiation field estimates in all transitions throughout the envelope, Monte Carlo energy packets are emitted from the core and their scattering histories are followed. The required memory for **Brute** is much larger than that for **Synow**, and **Brute** also lacks the speed of its

1D counterpart.

3.1. Synow Fits

Here we investigate a few spherically symmetric distributions of Ca II optical depth. The assumption of homology in the SN atmosphere ($v \propto r$) permits us to parameterize Sobolev optical depth in terms of velocity v relative to the explosion center. In spherical symmetry, we may designate domains $v_{min} < v < v_{max}$ within which we define reference line Sobolev optical depth according to the rule

$$\tau_{ref}(v) = \tau_{ref}(v_{min}) \exp[(v_{min} - v)/v_e] \quad (v_{min} < v < v_{max}), \quad (1)$$

where v_e is an *e*-folding length. If v_{min} is greater than the velocity at the photosphere v_{ph} , we say the optical depth profile is *detached*. Outside of the domain we may set the reference optical depth to zero, or use another rule for the same reference line to set up a superposition of optical depth profiles. Other line optical depths for the same ion are assigned assuming LTE excitation temperature T_{exc} . The velocity at the photosphere in all the presented Synow fits is $v_{ph} = 12500 \text{ km s}^{-1}$.

Synow uses a blackbody emitting photosphere, clearly insufficient to account for all real continuum processes at work in the formation of a SN spectrum. This limits the range over which the synthetic continuum level can be made consistent with that observed, making fits of entire spectra extending from 3000 Å to 10000 Å problematic. We adopt a piecewise approach and choose a convenient blackbody temperature applicable for the blue part of the spectrum. Fitting only the major features blueward of 6000 Å (excluding lines of Ca II), we find that a blackbody temperature $T_{bb} = 12000 \text{ K}$ yields a decent fit to this region. Since increasing T_{bb} from this value changes the continuum slope in the neighborhood of the IR triplet only slightly, we choose to merely scale the synthetic spectra down in order to fit that feature.

Except for the optical depth parameters of Ca II, the other parameters (v_{ph} , T_{bb} , and optical depths of ions listed in Table 1) stay fixed from fit to fit. Since the Ca II IR triplet may blend with some lines of O I, a small amount of optical depth for that ion is included in the fit, but its presence has little impact on the results. The parameters used for the various Ca II optical depths are listed in Table 2.

3.1.1. One-Component Fits

Here we present three illustrative fits of the Ca II features using only one spherically symmetric velocity component in each. Figure 3 shows an example of a fit to the entire spectrum range. The observed features between 4500 Å and 6000 Å are fit rather well assuming the parameters for Fe III, Si II, and S II given in Table 1.

In Figure 4 are close-ups of the H&K feature and IR triplet fits using model 1D1 from Table 2. This single-shell model with nearly constant optical depth as a function of radius can reproduce the broad velocity extent of the H&K feature. Yet it cannot reproduce any of the structure present in the IR triplet, so next we consider independent fits to the PV and HV features to investigate this structure.

The appearance of the two strongest IR triplet lines (Ca II $\lambda\lambda 8542, 8662$) in the PV feature as two distinct notches presents an interesting problem under spherical symmetry. In general, without assuming $v_{min} > v_{ph}$ or imposing a finite v_{max} , generating such a feature in spherical symmetry is only possible if $v_{ph} \lesssim v_{sep}$, where v_{sep} is the velocity separation of the two lines. To fit the Si II and Fe III features, $v_{ph} = 12500 \text{ km s}^{-1}$ is used, but v_{sep} for the two strongest IR triplet lines is only about 4000 km s^{-1} and both notches have minima wavelengths consistent with a 12500 km s^{-1} blueshift.

An alternative is to impose a finite v_{max} or small v_e that prevents blending of the two absorptions into one. But this has the undesirable effect of making absorptions with flat bottoms which (when combined together) generate a Ca II $\lambda 8542$ feature *shallower* than the redder line, even though the former has a higher oscillator strength. For the moment, we allow the features to blend into one absorption, using the parameters listed for fit 1D1PV in Table 2 which provide a satisfactory fit to the PV features in Figure 5.

Fitting the HV notches with a shell of Ca II optical depth (fit 1D1HV in Figure 6) is considerably less problematic than in the case of the PV feature. Using a small v_e or imposing a finite v_{max} prevents blending that would otherwise unite the two bluer notches of the IR triplet feature. However, the synthetic H&K feature seems much narrower than needed.

3.1.2. Two-Component Fit

Combining the one-component PV and HV fits described above yields fit 1D2 (Figure 7). This fit is satisfactory for the IR triplet, but its major deficiency is that the peak between the two blue notches is higher than observed. Adjusting v_{max} from 25000 km s^{-1} to higher

velocity permits the redder feature to weaken this peak, extends the bluest synthetic notch further to the blue than is desired. On the other hand, the synthetic H&K feature appears to need some higher-velocity material to extend its blue edge.

3.1.3. Three-Component Fit

Using three velocity components of Ca II optical depth allows us to fit every notch in the IR triplet absorption by simply overlapping pairs of notches formed by each component. The result of this model (1D3) is displayed in Figure 8. For the IR triplet, this appears to be the “best fit” among the 1D models, but the H&K feature is too strong in its bluest part. Imposing a finite v_{max} to counteract this HV tail only deepens the synthetic H&K absorption since it removes material that scatters light from the emission lobes of the envelope.

3.2. Brute Fit

The assumptions used in **Brute** are roughly the same as those in **Synow** except for the freedom to choose spatial optical depth distributions without spherical symmetry. Again the same blackbody emitting, sharp photosphere is assumed, resulting in the same continuum-level problem described before, and we use the same remedy here. The technique used for radiative transfer in **Brute** is that of Monte Carlo, a difference from **Synow**, but both codes take into account multiple scattering in the calculation of the source functions of the lines.

The spatial parameterization used for the Ca II optical depth consists of two components. One is spherical (PV material) and the other is not (HV material). The idea is to engineer a simple 3D distribution of optical depth that yields a synthetic spectrum consistent with observation, and fits at least as well as the 1D model.

For the HV material in the 3D fit, we adopt a simple geometry consisting of a circular cylinder of radius 8000 km s^{-1} coaxial with the line of sight to the center of the photosphere. The reference optical depth for Ca II inside the cylinder is assigned according to the rule

$$\tau_{ref}(v_z) = \begin{cases} 0.0225v_z - 441.0 & : 19600 < v_z < 22400 \text{ km s}^{-1} \\ -0.0315v_z + 768.6 & : 22400 < v_z < 24400 \text{ km s}^{-1}. \end{cases} \quad (2)$$

According to this rule, the optical depth in the cylinder reaches a maximum value of $\tau_{ref} = 63$ at the plane $v_z = 22400 \text{ km s}^{-1}$. Outside the cylinder, the optical depth for the Ca II reference line is prescribed by eq. (1) with $\tau_{ref}(v_{min}) = 7$, $v_e = 3000 \text{ km s}^{-1}$, and $v_{min} = 13000 \text{ km s}^{-1}$. A plot of reference optical depth along the line of sight is presented in Figure 9. The

reference optical depths of the other ions are parameterized exactly as in the Synow fits and produce the same features.

The Ca II features resulting from this 3D parameterization are shown in Figure 10. The fit to the HV IR triplet is rather good. The synthetic HV H&K is more consistent with the observation than in the 1D2 or 1D3 parameterizations. Since the PV Ca II optical depth is distributed much the same as in the 1D2 case, the observed peak between the redder notches cannot be reproduced. In the 1D case, this could only be accomplished by adding a third shell of optical depth and tuning its position. We note that in the 3D case, if the PV material is deployed in a nonspherical manner (such that parts of the photosphere shine through) then the peak between the two PV notches can be reproduced quite easily.

4. Discussion

4.1. HV Ejecta Geometry from the Fits

Reconstructing SN envelope structure from spectra is an ill-posed inverse problem. The problem becomes even more difficult when the assumption of spherical symmetry is relaxed; the presented 3D solution represents but one of many possible solutions.

In fact, to first order, any HV distribution of Ca II optical depth which yields the same photospheric covering factor as a function of v_z will produce the same absorption features. The most promising avenue for breaking this degeneracy is through synthetic spectropolarimetry of high-quality data. The Stokes polarization parameters Q and U for wavelengths covering the Ca II features are required. Such Q-U plots are the means by which the HV ejecta geometry of SN 2001el is constrained (Kasen et al. 2003).

Both that study and the present one focus on the absorption features of Ca II, and ignore the emission features. Generally, emission phenomena are of limited utility in assessing HV ejecta geometry. In spherical symmetry, a HV shell gives rise to a weak, flat-topped emission feature barely detectable in flux spectra. On the other hand, if the HV ejecta are organized into isolated regions of high optical depth, those not covering the photosphere along the line of sight will only contribute individual emission bumps to the spectrum. These weak features are even harder to detect if the PV ejecta are spherically symmetric and contribute significantly to the emission feature.

On the practical side, the peculiarities of the spectrum of SN 2000cx make it impossible to use the Ca II emission features for geometrical analysis. The H&K emission feature is disrupted by a sequence of narrow lines, while the IR triplet emission is plagued by noise.

These factors (the inherent degeneracies of the problem, the lack of corroborating polarization data, the limited utility of emission features) prevent us from making all but the most conservative statements about the HV ejecta geometry of SN 2000cx. The similarity of the HV IR triplet of SN 2000cx to that of SN 2001el is suggestive, and its geometrical interpretation in the latter event motivates our consideration of a 3D model for SN 2000cx.

From a purely empirical standpoint, none of the presented fits stands out as the “best” overall. Any cosmetic details missed by the synthetic spectra could be tuned away by making minor adjustments to the models. However, the main goal is to simultaneously fit the HV H&K and IR triplet, and the 3D fit seems to do a better job.

Regardless of the details of the true geometry of the HV Ca II in SN 2000cx, the presence of this feature in only some SNe Ia evokes a series of questions to address in the future as high-quality data become available and 3D spectrum analysis techniques improve.

(1) How frequent is HV ejecta clumping in SNe Ia? All SNe Ia might possess HV deviation from spherical symmetry which could escape detection if optically thick parts did not obscure the photosphere. SNe 2001el and 2000cx might be examples where fortuitous orientation of HV ejecta permitted detection. This explanation is bolstered by the otherwise normal appearance of the SN 2001el spectrum. However, the peculiarities of SN 2000cx (the Fe III lines in its spectrum, its unusual light curve and color evolution; Li et al. 2001) make this hypothesis somewhat problematic.

(2) What implication does the presence of clumpy HV ejecta have for explosion models? If some SNe Ia have nonspherical HV ejecta while others do not, it might imply that more than one progenitor model is needed to explain the SN Ia phenomenon. More conservatively, the clumpiness of the HV ejecta might be a consequence of a so-called second parameter (Branch 2001).

(3) Does the existence of nonspherical SNe Ia influence the prospects for precision SN cosmology? The most obvious spectroscopic effect would be due to the application of spherical K-corrections to nonspherical events. This effect is probably minor unless the consequences for spectrum formation from geometry appear in more than just a few lines.

Ca II lines are notoriously excitable over a large range of temperature and density. This makes it possible to place limits on the HV ejecta mass, and in turn to constrain future white dwarf explosion models.

4.2. HV Ejecta Mass Estimates

Here we make some simple estimates of the HV ejecta mass as constrained by the Ca II features visible in the SN 2000cx spectrum at two days after maximum light. We make four pairs of estimates, each pair consisting of a 1D and 3D measurement. The first pair of estimates is made for the extreme case of a purely calcium HV ejecta composition. The second pair is based on a C/O-rich composition, similar to the outer, unburned layers of a white dwarf. Since the HV material may be possibly stripped material from a main-sequence or red-giant companion of the progenitor (Marietta et al. 2000), we use a H-rich composition for a third set of estimates. Finally, since recurrent nova models (a possible channel for SN Ia production; Hachisu et al. 1999) include helium stars as companions, we consider the case of a He-rich composition. These last three compositions (C/O-rich, H-rich, and He-rich) are as listed in the ion signatures atlas of Hatano et al. (1999b).

For each pair of estimates, we adopt the 1D2 and 3D parameterization domains for the volume used in calculating the HV ejecta mass. These are

$$\begin{aligned} V_{HV}^{1D2} &= 3.9 \times 10^{46} \text{ cm}^3, \\ V_{HV}^{3D} &= 5.0 \times 10^{45} \text{ cm}^3. \end{aligned} \quad (3)$$

These presented mass estimates are not intended to be exact; in all cases the assumption of LTE is employed. More rigorous constraints on the HV ejecta mass require detailed modelling of the physical conditions in the HV material, and these will be the focus of much future work. The estimates here and in Kasen et al. (2003) are a starting point for that effort.

4.2.1. Pure Calcium Composition

In the Sobolev approximation, line optical depth for a transition $l \rightarrow u$ in a SN envelope is given by (Jeffery & Branch 1990)

$$\tau_{lu} = \frac{\pi e^2}{m_e c} f_{lu} \lambda_{lu} n_l t \left(1 - \frac{g_l n_u}{g_u n_l} \right), \quad (4)$$

where f_{lu} is the oscillator strength, λ_{lu} is the transition wavelength, n_l and n_u are the lower and upper level occupation number densities respectively, and t is the time since explosion. The other symbols have their usual meanings. For convenience, we rewrite this as

$$\tau_{lu} = 2.292 \times 10^{-5} (gf)_{lu} \lambda_{\text{A}} n t_d \frac{\exp(-E_l/kT)}{Q(T)}, \quad (5)$$

where we have neglected the correction factor for stimulated emission, replaced the constants with their numerical values, and imposed LTE. The LTE partition function $Q(T)$ for the ion in question is included.

If the HV ejecta consist of singly ionized calcium in the ground state, then the optical depth in the Ca II $\lambda 3934$ transition (the reference line) becomes roughly proportional to the mass density of the HV ejecta. In reality, the gas consists of other ions of calcium and other species, so deriving a mass density assuming a pure Ca II composition provides an extreme lower limit to the HV mass. Substituting $\lambda_{\text{A}} = 3934$, $(gf)_{3934} = 1.3614$, $E_l = 0$ eV, and $t_d = 20$ into eq. (5) gives

$$\tau_{3934} \simeq 2.46 n_{\text{CaII}} / Q(T). \quad (6)$$

If we assume that the temperature in the HV ejecta is less than 8000 K, we can use the simple approximation $\tau_{3934} \simeq n_{\text{CaII}}$ since $Q(T)$ varies slowly from 2 to 3 up to 8000 K.

Now an average mass density for the HV ejecta as derived from the Ca II optical depth can be written

$$\langle \rho_{\text{HV}} \rangle \simeq (A_{\text{Ca}}/N_{\text{Avogadro}}) n_{\text{Ca}} \simeq 6.66 \times 10^{-23} \langle \tau_{\text{HV}} \rangle \text{ g cm}^{-3}. \quad (7)$$

If we average the reference line optical depths over the 1D2 and 3D parameterization domains, then $\langle \tau_{\text{HV}}^{1D2} \rangle = 25.5$ and $\langle \tau_{\text{HV}}^{3D} \rangle = 31.5$. Substituting these values into eq. (7) and multiplying by the volume in each case,

$$\begin{aligned} M_{\text{HV}}^{1D2} &\gtrsim 3.3 \times 10^{-8} M_{\odot}, \\ M_{\text{HV}}^{3D} &\gtrsim 5.2 \times 10^{-9} M_{\odot}. \end{aligned} \quad (8)$$

These mass estimates are the “rock bottom” numbers required for the observational signature of the Ca II $\lambda 8542$ line. The deflagration model W7 (Nomoto et al. 1984; Branch et al. 1985) suggests that the amount of material and the densities in this region should be much higher, on the order of $6.0 \times 10^{-3} M_{\odot}$ in spherical symmetry above 20000 km s⁻¹. Including other species into the mass calculations improves the lower limit, but this requires a choice of a particular composition.

4.2.2. C/O-Rich Composition

A more realistic composition model than that of pure calcium can be used to produce a more meaningful constraint on the HV ejecta mass. Here we adopt the C/O-rich composition from the ion signature atlas of Hatano et al. (1999b) as the candidate model. This composition is representative of the unburned outer layers of an exploded white dwarf.

The procedure for constraining the HV mass density is quite simple. First we solve the LTE equation of state for a range of values of temperature T and density ρ_{tot} . Then we find regions of the $T - \rho_{tot}$ plane for which the optical depth of Ca II $\lambda 8542$ exceeds unity. The lowest total mass density for which this line has a non-negligible optical depth will provide a lower limit to the HV mass density, and from this we derive a lower limit to the HV ejecta mass.

Contours of $\tau = 1$ for Ca II $\lambda 3934$ and $\lambda 8542$ are shown in Figure 11. For the C/O-rich composition, the absolute minimum mass for which Ca II $\lambda 8542$ has a spectroscopic signature is at $\rho_{min}^{C/O} = 2.2 \times 10^{-16} \text{ g cm}^{-3}$. This density is marked by a dotted vertical line.

The value of $\rho_{min}^{C/O}$ depends on the choice of T , as does the relative strength of Ca II $\lambda 8542$ to $\lambda 3934$. However, since the optical depth of Ca II $\lambda 3934$ is always much greater than that of the IR line, it is difficult to constrain the exact value of T in the HV ejecta using this technique. As τ in a line approaches ∞ , the line profile saturates and the dependence of the absorption feature depth on τ disappears. Rather than resort to predictions from detailed models for a temperature in the HV ejecta, we adopt the absolute minimum value given above for a conservative LTE estimate of the HV ejecta masses:

$$\begin{aligned} M_{HV}^{1D2} &\gtrsim 4.3 \times 10^{-3} M_{\odot}, \\ M_{HV}^{3D} &\gtrsim 5.5 \times 10^{-4} M_{\odot}. \end{aligned} \quad (9)$$

These mass estimates and densities are roughly consistent with the W7 estimate of $6.0 \times 10^{-3} M_{\odot}$ in spherical symmetry above 20000 km s^{-1} . This might suggest that the Ca II signature could arise from primordial material as was suggested for SN 1994D (Hatano et al. 1999a), rather than from freshly synthesized material.

As the density increases from $\rho_{min}^{C/O}$, lines of Ti II, Sr II, and Fe II should appear for higher temperatures, while lines of Fe I and Ca I should appear at lower temperatures, as seen in Figure 12. The lower-excitation lines are certainly missing from the spectrum, but the identification of lines from the higher ionization stages is problematic. The Ti II lines could be present to the blue of the 4300 \AA Fe III feature, but this identification is uncertain. Sr II lines from HV ejecta blend with the Ca II H&K feature. Fe II lines would be heavily blended with the Fe III features. These uncertainties prevent us from using Figure 12 to cap the value of $\rho_{HV}^{C/O}$.

4.2.3. Other Compositions

Marietta et al. (2000) present very interesting simulations of the effect that a white dwarf in a binary has on its companion when it explodes. Generally, they note that more evolved

companions (with less tightly bound envelopes) are more vulnerable to losing a substantial fraction of their envelope during the explosion. The resulting ejecta distribution includes an evacuated cone in the ejecta behind the companion and some hydrogen with characteristic velocity on the order of 1000 km s⁻¹. However, a small amount of stripped hydrogen (about $10^{-4}M_{\odot}$) could be carried up to velocities above 15000 km s⁻¹. Could the HV Ca II lines be a signature of this material?

We repeat the previous mass estimate calculation assuming a H-rich composition. The $\tau = 1$ contour plot for Ca II $\lambda 3934$ and $\lambda 8542$ is shown in Figure 13 along with $\tau = 1$ contours of H α and H β . The absolute minimum density for which the Ca II $\lambda 8542$ optical depth is significant in the H-rich case is $\rho_{min}^H = 3.2 \times 10^{-16}$ g cm⁻³, 45% higher than in the C/O-rich case. This results in lower limit masses of

$$\begin{aligned} M_{HV}^{1D2} &\gtrsim 6.2 \times 10^{-3} M_{\odot}, \\ M_{HV}^{3D} &\gtrsim 8.0 \times 10^{-4} M_{\odot}. \end{aligned} \quad (10)$$

These estimates are about an order of magnitude larger than the ($\sim 10^{-4}M_{\odot}$) HV ejecta masses predicted by Marietta et al. If those simulations are correct, these mass estimates seem to point to another origin for the HV ejecta.

However, we reiterate the simplistic nature of our HV ejecta model. Since only flux spectra are available for SN 2000cx, we cannot place firm constraints on the HV ejecta volume. If this volume were to be decreased somewhat and the estimates of HV mass by (Marietta et al. 2000) are too low, the answer might be different.

A serious concern for the H-rich model composition is that H α may become detectable in the HV ejecta if the density is much higher than ρ_{min}^H . In fact, the lowest density for which the H α optical depth exceeds unity is 1.2×10^{-15} g cm⁻³, and the lowest density for which H β exceeds unity is 3.7×10^{-15} g cm⁻³. There is one unidentified absorption feature at about 4500 Å which could be HV H β . In Figure 14 we show a fit which includes H optical depth. In this model, the H optical depth is confined to the cylinder specified in eq. (2), but the optical depth in the reference line (H α) is $\tau_{ref} = 4$ at $v_z = 22400$ km s⁻¹ and drops to 0 at the cylinder faces. This geometry only partially covers the photosphere along the line of sight. This saturates the strength of the H α absorption and makes for its easy concealment by the Si II 6150 Å absorption feature. The agreement between the synthetic observed spectra is tantalizing.

If we insist that the 4500 Å feature is in fact due to H β , then the total mass density estimate increases so, that the HV ejecta masses are given by the following rather large

numbers which are clearly inconsistent with the (Marietta et al. 2000) findings:

$$\begin{aligned} M_{HV}^{1D2} &\gtrsim 7.2 \times 10^{-2} M_{\odot}, \\ M_{HV}^{3D} &\gtrsim 9.3 \times 10^{-3} M_{\odot}. \end{aligned} \quad (11)$$

Of course, the identification of $H\beta$ in the spectrum could be spurious. This would mean that the velocity overlap of the ejecta giving rise to the HV calcium and the purported hydrogen features is pure coincidence. Clearly other candidates must be investigated thoroughly, but we have found no less extraordinary line to produce this feature. This topic will be addressed in a future paper (D. Branch et al., in preparation).

A map of ion signatures for the H-rich composition appear in Figure 15 with the same density levels marked as in Figure 13. At about the same temperature and densities for which $H\beta$ becomes visible, we expect Ti II lines and Cr II (as well as Ca II). The HV Cr II lines appear blueward of 3500 Å, generally as one large feature, but this identification is made speculative due to the blue spectrum cutoff. Again, the identification of Ti II in the spectrum is at best uncertain.

One possible evolutionary track toward the production of a SN Ia is through recurrent novae (Starrfield 2003) or supersoft x-ray sources (Hachisu et al. 1999). These progenitors involve a He-rich (and H-deficient) companion star. To account for this possibility, we made a mass estimate using the He-rich composition from Hatano et al. (1999b) and arrive at roughly the same lower density limit for the signature of Ca II $\lambda 8542$ as in the H-rich case. Thus, the HV ejecta mass estimates for the He-rich case are about the same as listed in Equation (10). Since helium stars are more a (Marietta et al. 2000) scenario for this class of star seems even more unlikely to give rise to the observed HV Ca II features, therefore we suspect the material is produced in the explosion itself.

5. Conclusions

We have presented several exploratory fits to the unique Ca II features of the unusual SN Ia 2000cx. A 1D shell of material can account for the HV IR triplet feature, but has difficulty doing so for the corresponding H&K feature. In 3D, both HV features can be fit simultaneously with a chunk of material along the line of sight which partially covers the photosphere.

Mass estimates (assuming a C/O-rich composition) for the HV material in both geometries is consistent in the lower limit with the W7 model, suggesting a possible primordial origin. If the composition of the HV ejecta is H-rich or He-rich, more mass is required for the HV IR Ca II signature, exceeding that predicted by previous numerical simulations of

stripping of companion stars by SNe Ia. While the material could be swept up circumstellar material, no donor scenario predicts enough material in the circumstellar region to account for the optical depths we find.

Though it could be coincidental, we point out that a 4500 Å absorption feature can be fit by placing hydrogen optical depth in the same 3D configuration as the Ca II optical depth. This produces a blueshifted HV “H β ” feature at about 4500 Å and an H α feature concealed in the Si II 6150 Å absorption. Alternative explanations for this feature will be discussed in detail in a forthcoming direct analysis paper (D. Branch et al., in preparation).

Understanding the origin of the HV ejecta in SNe Ia (and also its frequency and physical conditions) is potentially quite important for future explosion models and for answering the progenitor question. It is clear that better constraints on the HV Ca II phenomenon require high-quality maximum light flux and polarization spectra at near-infrared and near-ultraviolet wavelengths.

The authors acknowledge other members of the University of Oklahoma SN Group, Dan Kasen and Peter Nugent, for their helpful comments. The research presented in this article made use of the SUSPECT⁴ Online Supernova Spectrum Archive, and the atomic line list of R. L. Kurucz (Kurucz 1993). This work has been supported by grant HST-AR-09544-01.A (provided by NASA through the STScI, operated by the AURA, Incorporated, under NASA contract NAS5-26555), NASA grant NAG5-12127, and NSF grants AST-9986965, AST-9987438, and AST-0204771.

REFERENCES

Baron, E., et al. 2000, ApJ, 545, 444

Branch, D. 2001, PASP, 113, 169

Branch, D., et al. 2002, ApJ, 566, 1005

Branch, D., Doggett, J., Nomoto, K., & Thielemann, F-K. 1985, ApJ, 294, 619

Castor, J. 1970, MNRAS, 149, 111

Fisher, A. 2000, Ph. D. Thesis, University of Oklahoma

⁴<http://www.nhn.ou.edu/~suspect>

Gamezo, V., Khokhlov, A., Oran, E., Chtchelkanova, A., & Rosenberg, R. 2003, *Science*, 299, 77

Hachisu, I., Kato, M., Nomoto, K., & Umeda, H. 1999, *ApJ*, 519, 314

Hatano, K., Branch, D., Fisher, A., Baron, E., & Filippenko, A. V. 1999a, *ApJ*, 525, 881

Hatano, K., Branch, D., Fisher, A., Millard, J., & Baron, E. 1999b, *ApJS*, 121, 223

Hauschildt, P., & Baron, E. 1999, *J. Comp. Applied Math.*, 109, 41

Hillebrandt, W., Reinecke, M., & Niemeyer, J. 2000, *astro-ph/0012072*

Howell, D., Höflich, P., Wang, L., & Wheeler, J. 2001, *ApJ*, 556, 302

Jeffery, D., & Branch, D. 1990, in *Jerusalem Winter School for Theoretical Physics*, Vol. 6, *Supernovae*, ed. J. C. Wheeler, T. Piran & S. Weinberg (Singapore: World Scientific), 149

Kasen, D., et al. 2003, *ApJ*, submitted, (*astro-ph/0301312*)

Khokhlov, A., 2000, *astro-ph/0008463*

Kurucz, R. 1993, CD-ROM 1, *Atomic Data for Opacity Calculations* (Cambridge: Smithsonian Astrophysical Observatory)

Li, W., et al. 2001, *PASP*, 113, 1178

Marietta, E., Burrows, A., & Fryxell, B. 2000, *ApJS*, 128, 615

Mazzali, P., & Lucy, L. 1993, *A&A*, 279, 447

Millard, H., et al. 1999, *ApJ*, 527, 746

Nomoto, K., Thielemann, F-K., & Yokoi, K. 1984 *ApJ*, 286, 644

Sobolev, V. 1947, *Moving Envelopes of Stars* (Leningrad: Leningrad State University) (English transl. S. Gaposchkin [Cambridge: Harvard University Press, 1960])

Starrfield, S. 2003, in *From Twilight to Highlight: The Physics of Supernovae*, ed. W. Hillebrandt & B. Leibundgut, in press

Thomas, R., Kasen, D., Branch, D., & Baron, E. 2002, *ApJ*, 567, 1037

Table 1. Synow Fit Parameters for Non-Calcium Ions

Ion	$\tau_{ref}(v_{min})$	v_{min}	v_{max}	v_e	T_{exc}
		(10^3 km s $^{-1}$)	(10^3 km s $^{-1}$)	(10^3 km s $^{-1}$)	(10^3 K)
Fe III	1.5	12.5	∞	1.0	10.0
Si II	3.5	12.5	∞	1.0	10.0
S II	1.5	12.5	∞	1.0	10.0
O I	0.2	12.5	∞	3.0	8.0

Table 2. Synow Ca II Fit Parameters

Fit	(Figure)	Number of Components	$\tau_{ref}(v_{min})$	v_{min} (10^3 km s $^{-1}$)	v_{max} (10^3 km s $^{-1}$)	v_e (10^3 km s $^{-1}$)	T_{exc} (10^3 K)
1D1	(4)	1	1.4	12.5	30.0	20.0	8.0
1D1PV	(5)	1	10.0	12.5	∞	3.0	8.0
1D1HV	(6)	1	20.0	24.0	∞	0.5	8.0
1D2	(7)	2	10.0	12.5	24.0	3.0	8.0
			30.0	24.0	25.0	3.0	8.0
1D3	(8)	3	16.0	13.0	15.1	3.0	8.0
			7.0	19.0	23.5	3.0	8.0
			12.0	23.5	∞	3.0	8.0

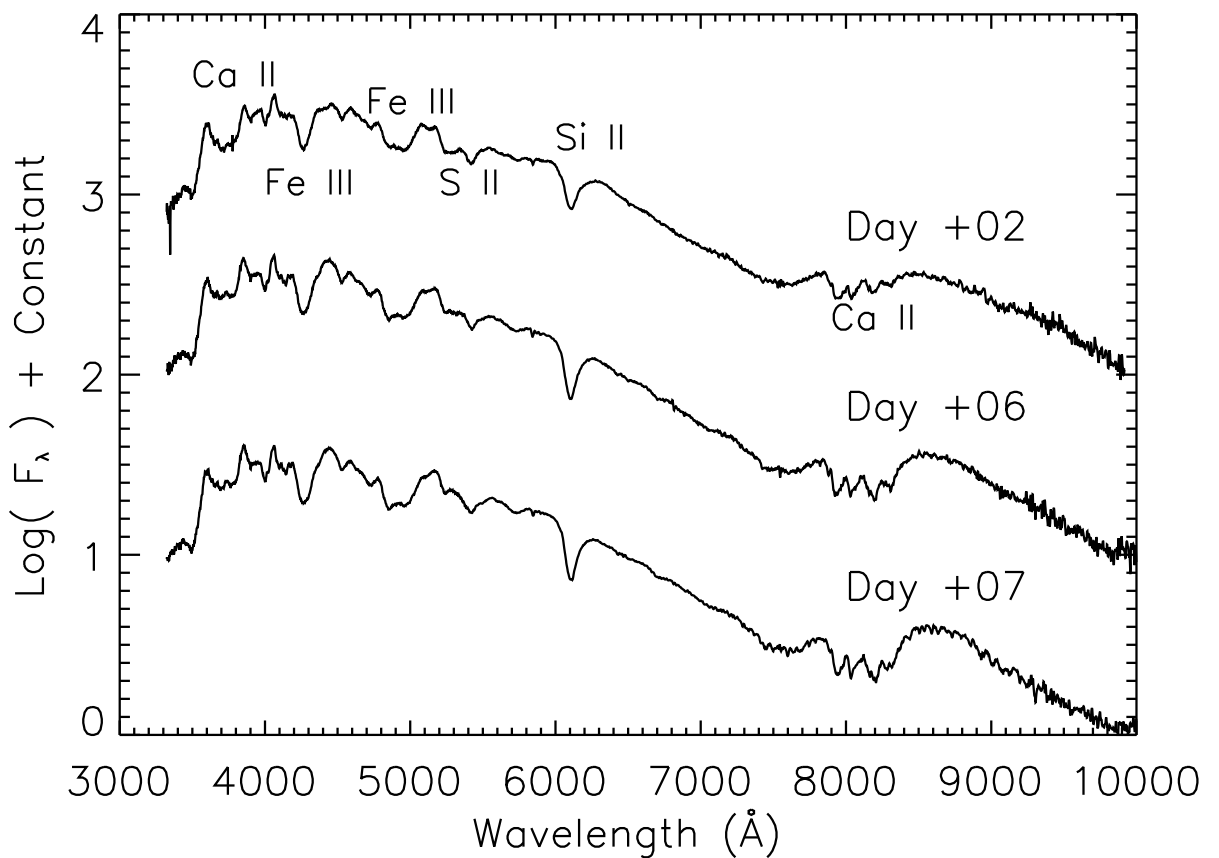


Fig. 1.— Near-maximum light spectra of SN 2000cx (Li et al. 2001). The epoch relative to maximum light is listed above each spectrum.

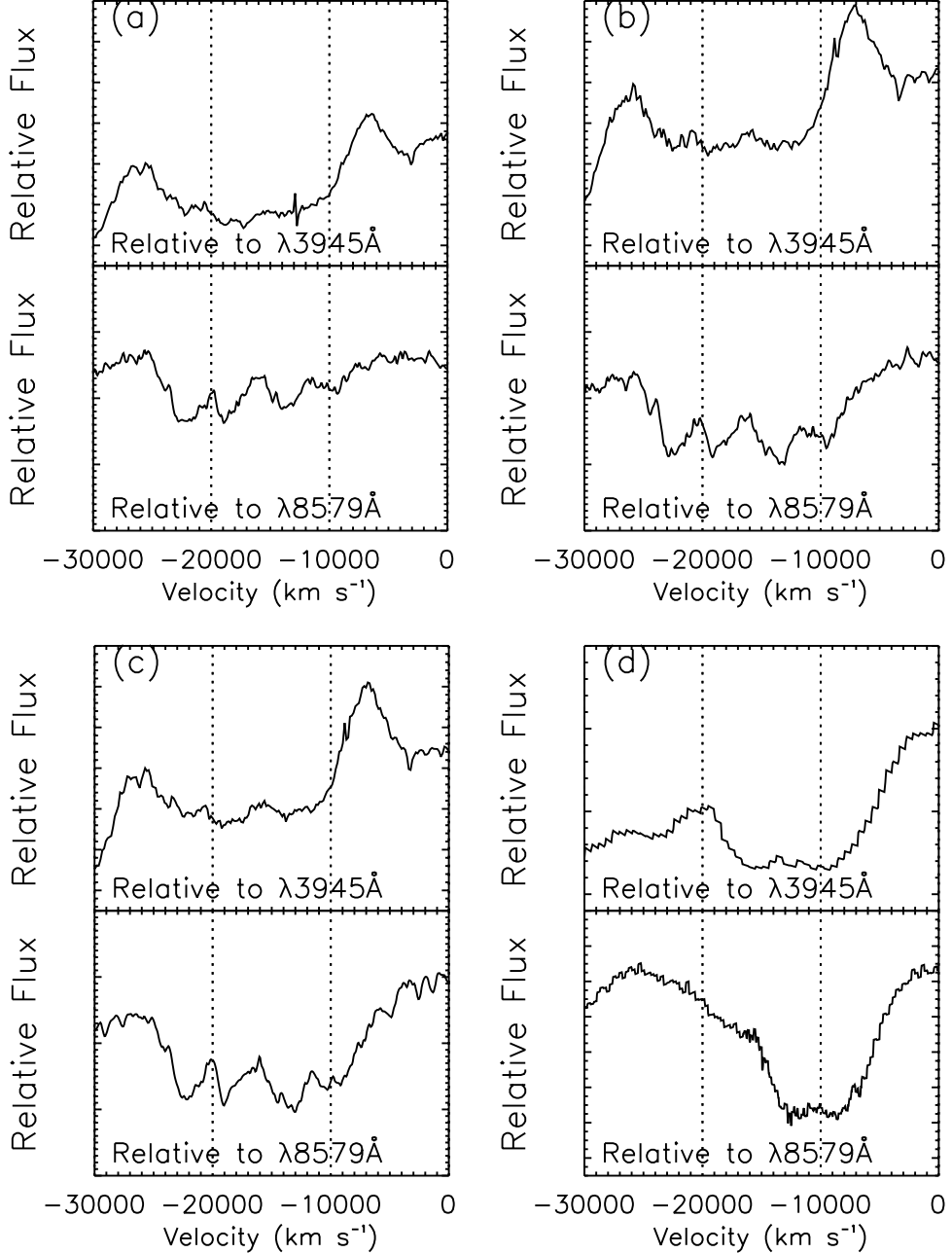


Fig. 2.— Ca II features in SN 2000cx at days 2 (a), 6 (b), and 7 (c) after maximum light, and those in SN 1994D at day 3 (d) after maximum. The features are plotted in terms of velocity relative to the observer, using the *gf*-weighted wavelengths of the Ca II H&K and IR triplet features.

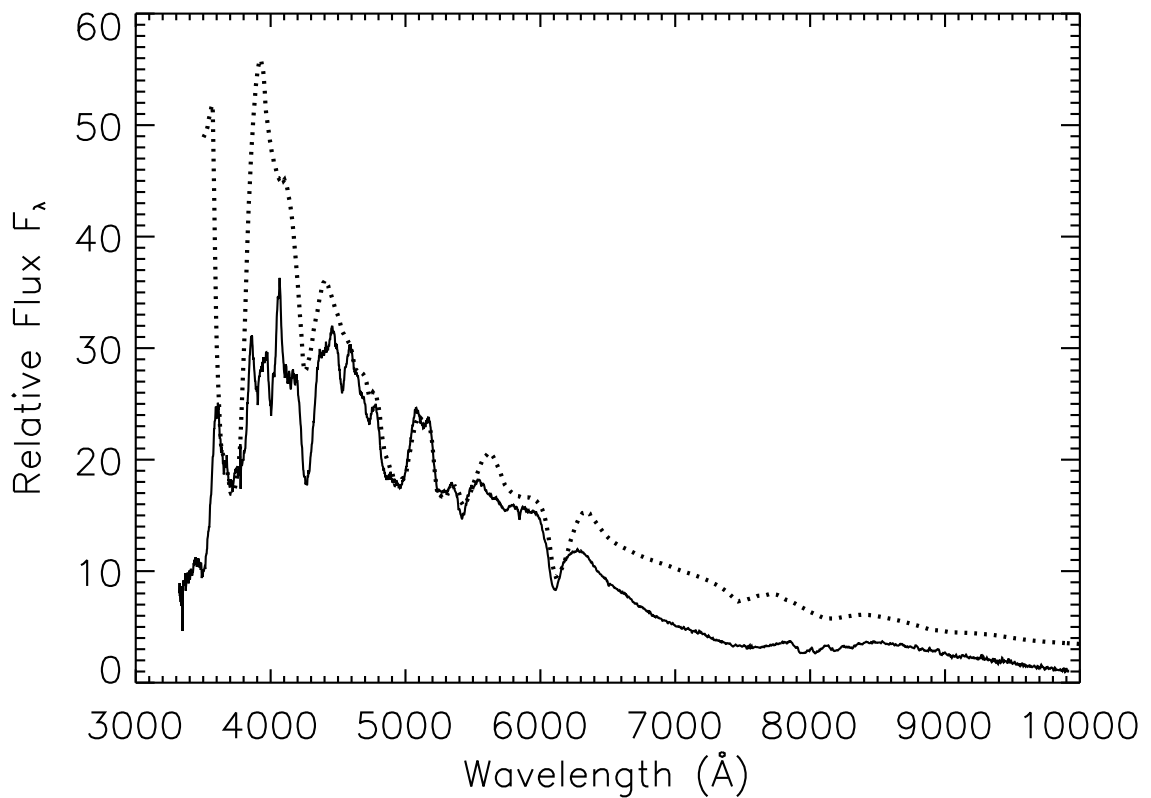


Fig. 3.— *Synow* fit 1D1 (dotted line) of SN 2000cx (solid line) two days after maximum with one Ca II component. Optical depths and excitation temperatures used for the other ions (Fe III, Si II, S II, and O I) are as listed in Table 1.

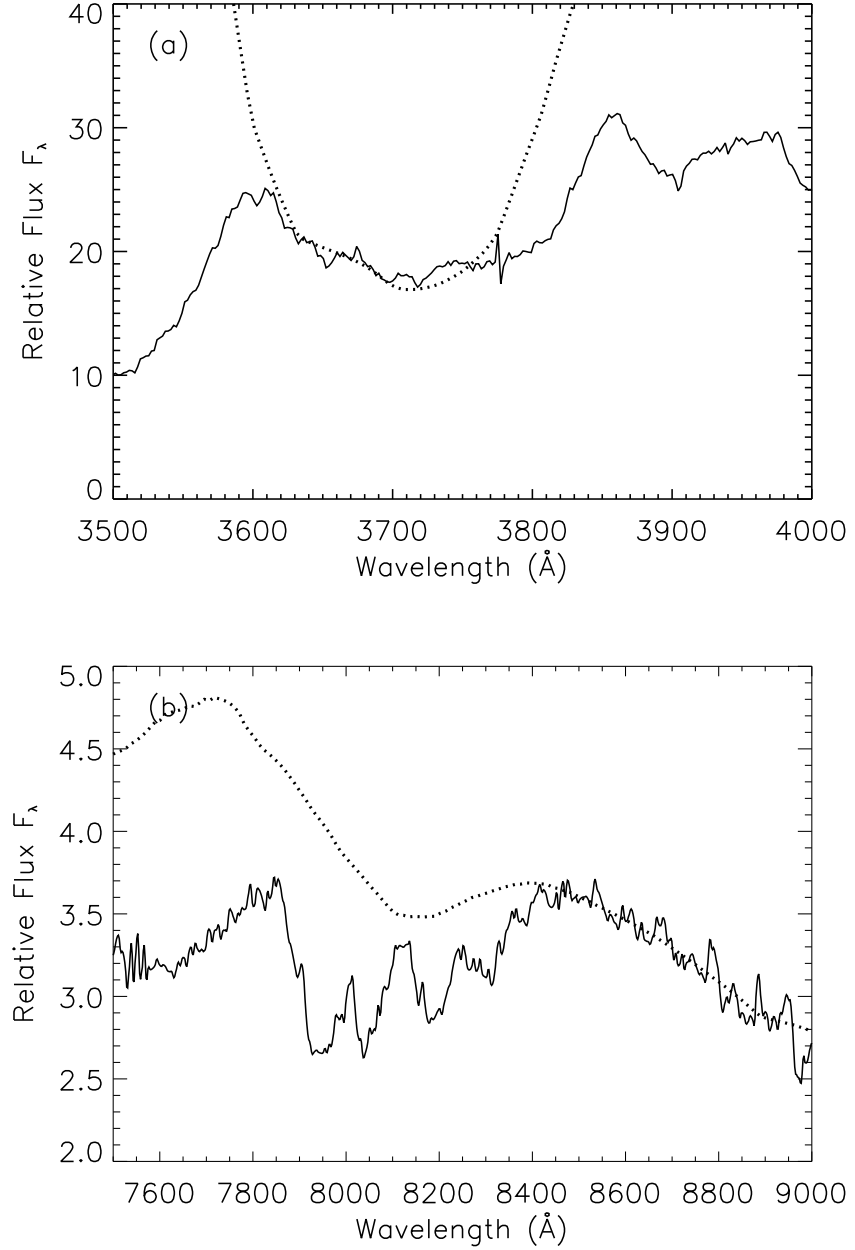


Fig. 4.— Synew fit 1D1 (dotted line) of Ca II features in SN 2000cx (solid line) two days after maximum. A single, nearly constant optical depth shell extending from the photosphere to 30000 km s^{-1} is used. The velocity extent of Ca II H&K is approximately reproduced, but the synthetic IR triplet lacks any of the structure seen in the observed spectrum.

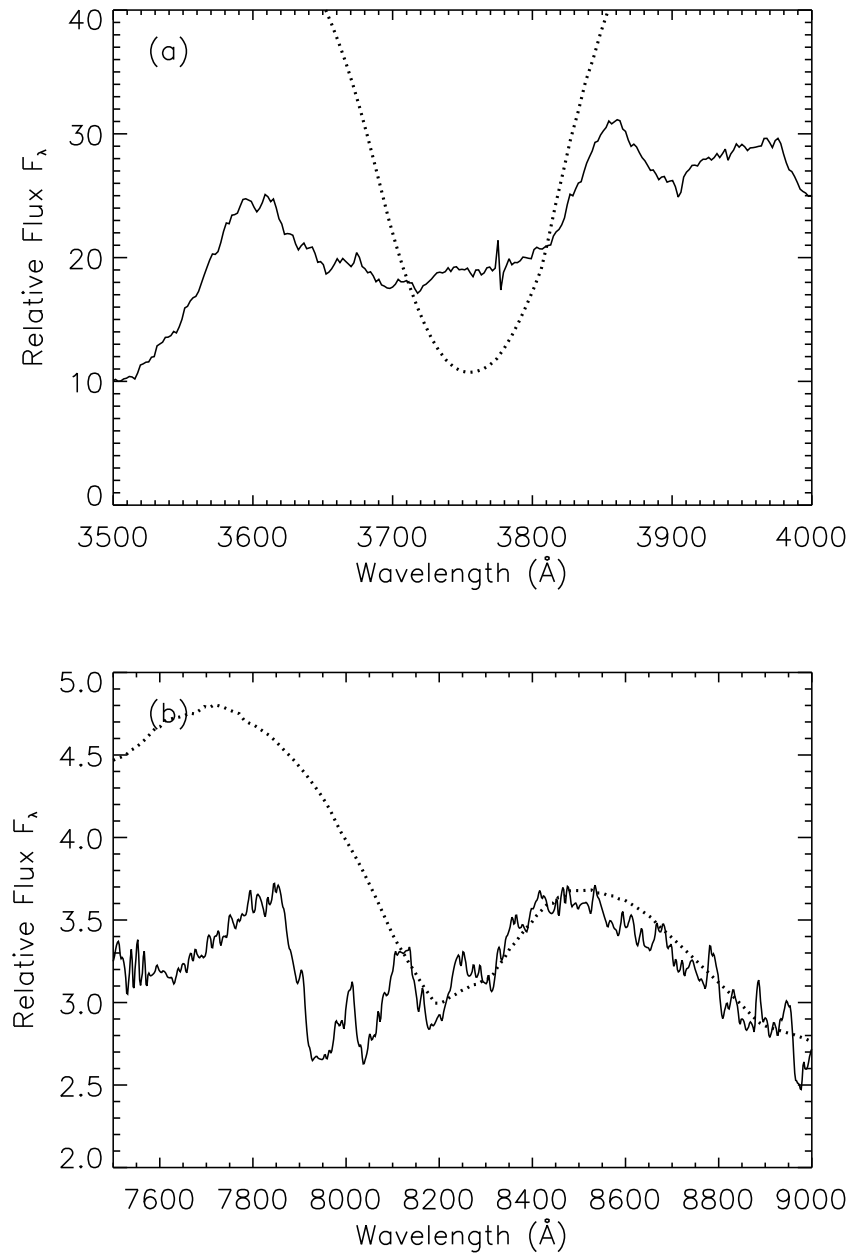


Fig. 5.— Synow fit 1D1PV (dotted line) of Ca II features in SN 2000cx (solid line) two days after maximum. A single, exponentially decreasing optical depth component just above the photosphere is used.

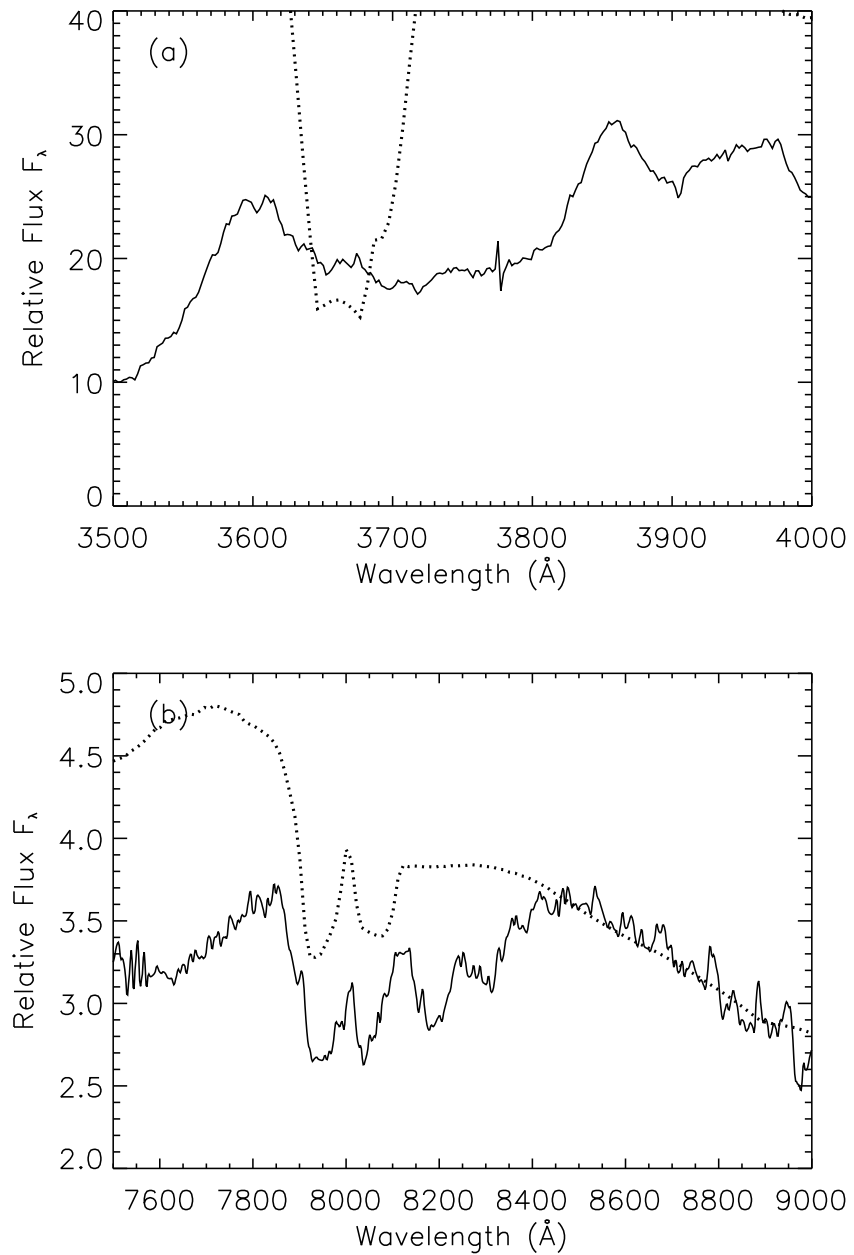


Fig. 6.— Synow fit 1D1HV (dotted line) of Ca II features in SN 2000cx (solid line) two days after maximum. A single, exponentially decreasing optical depth component at 20000 km s⁻¹ is used. An extremely small *e*-folding velocity of 500 km s⁻¹ is needed to prevent blending.

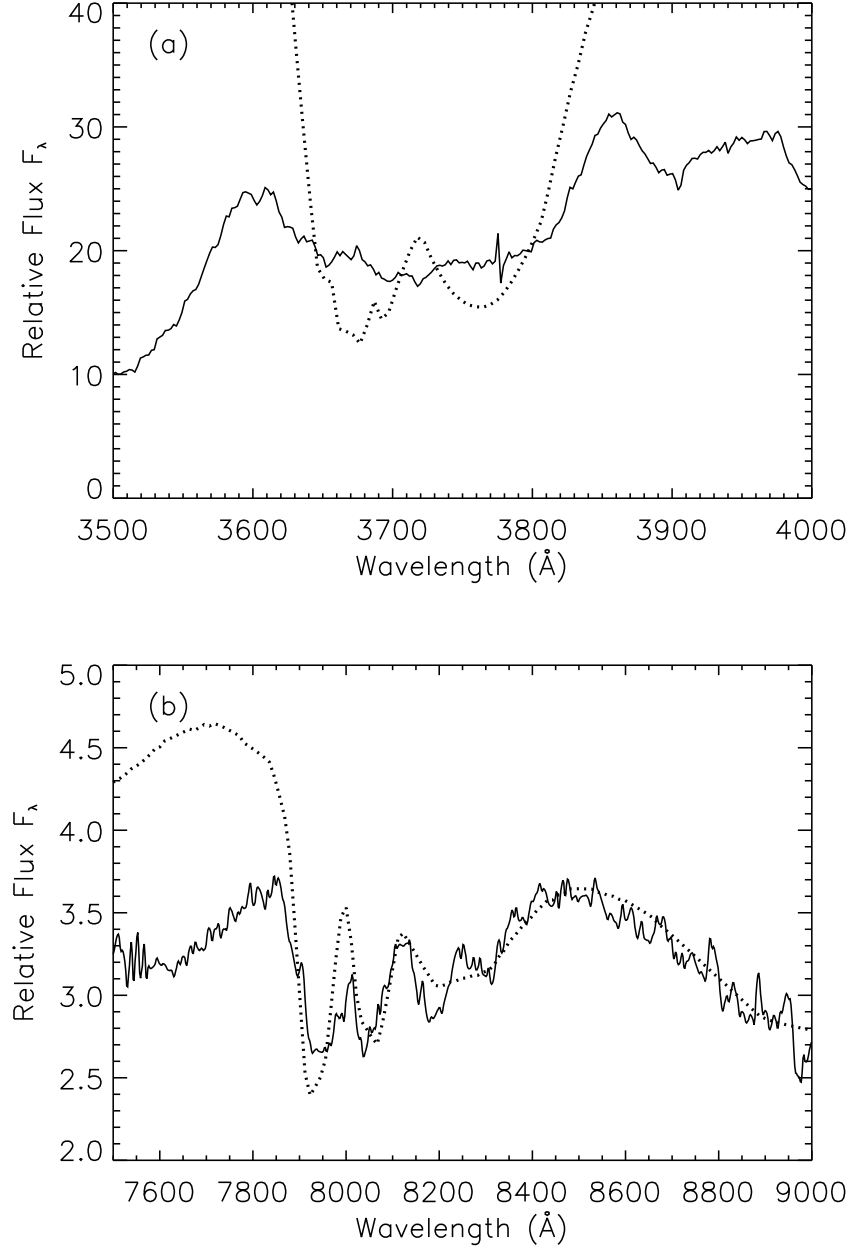


Fig. 7.— Synow fit 1D2 (dotted line) of Ca II features in SN 2000cx (solid line) two days after maximum. Two exponentially decreasing shells of Ca II optical depth are used. One extends from the photosphere to 24000 km s^{-1} and the other from 24000 km s^{-1} to 25000 km s^{-1} .

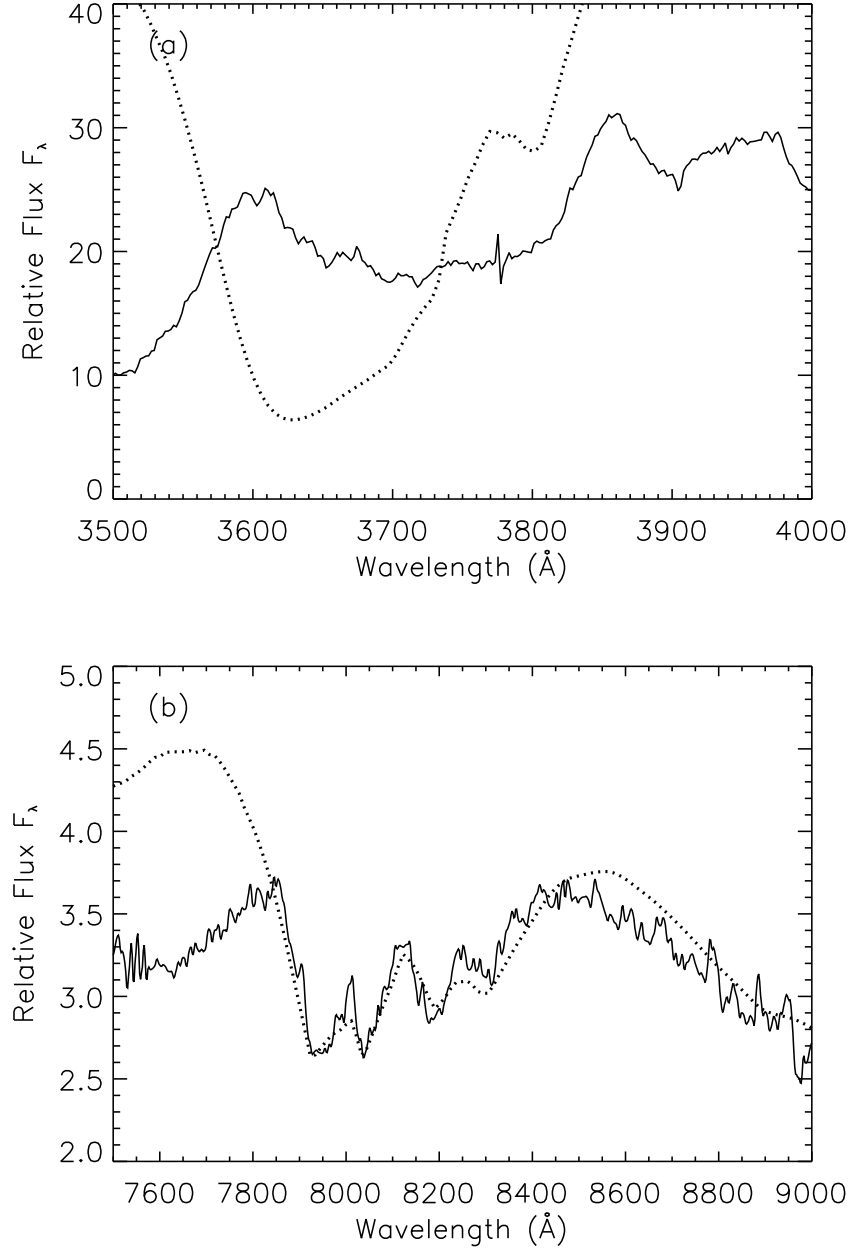


Fig. 8.— Synow fit 1D3 (dotted line) of Ca II features in SN 2000cx (solid line) two days after maximum. Three exponentially decreasing shells of Ca II optical depth are used to generate the peak between the two red notches of the triplet. The synthetic H&K feature is too strong compared to the observed one.

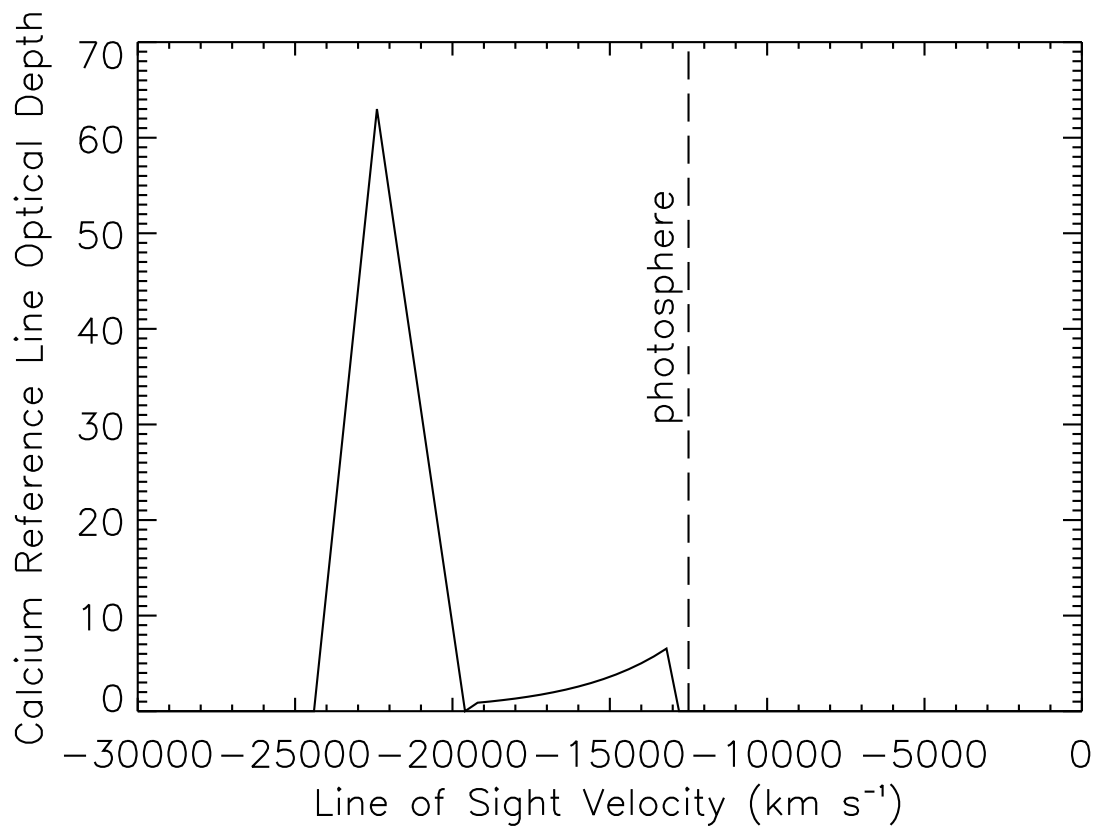


Fig. 9.— Ca II reference line optical depth along the $-z$ axis in the 3D model.

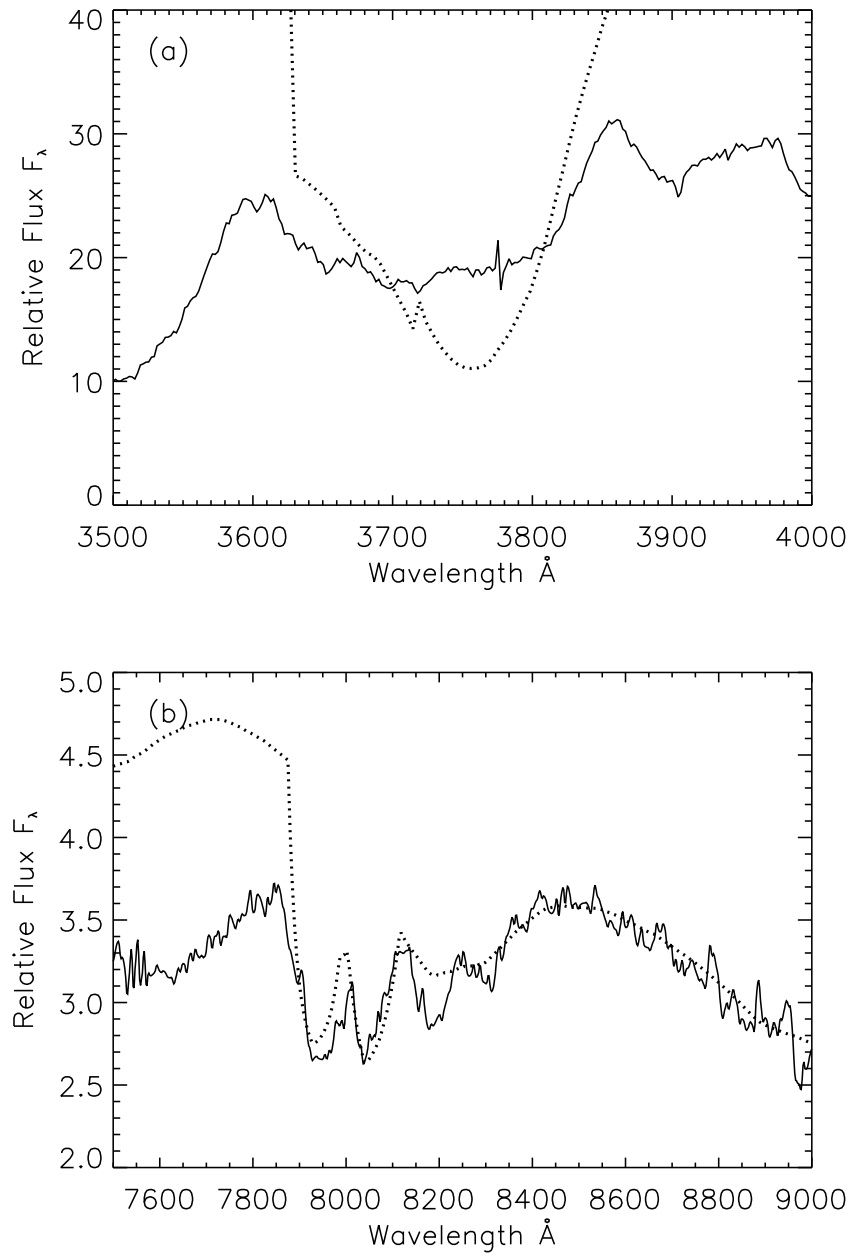


Fig. 10.— `Brute` fit (dotted line) of Ca II features in SN 2000cx (solid line) two days after maximum. The IR triplet is fit, and the blue edge of the synthetic H&K feature is weakened with respect to fit 1D3.

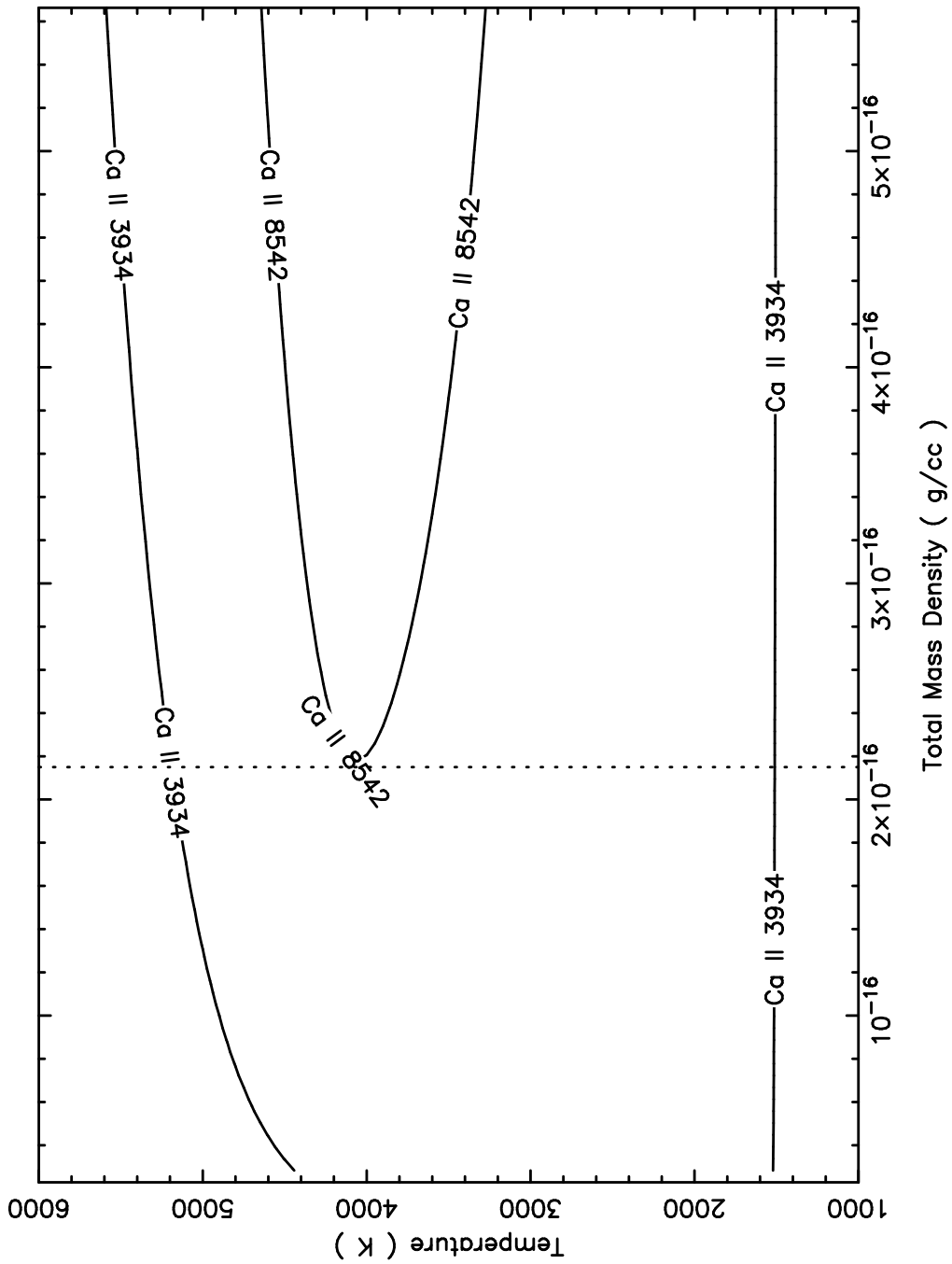


Fig. 11.— Contours of $\tau = 1$ for Ca II $\lambda 3934$ and $\lambda 8542$, assuming the C/O-rich composition. The dotted line denotes $\rho_{min}^{C/O} = 2.2 \times 10^{-16}$ g cm $^{-3}$.

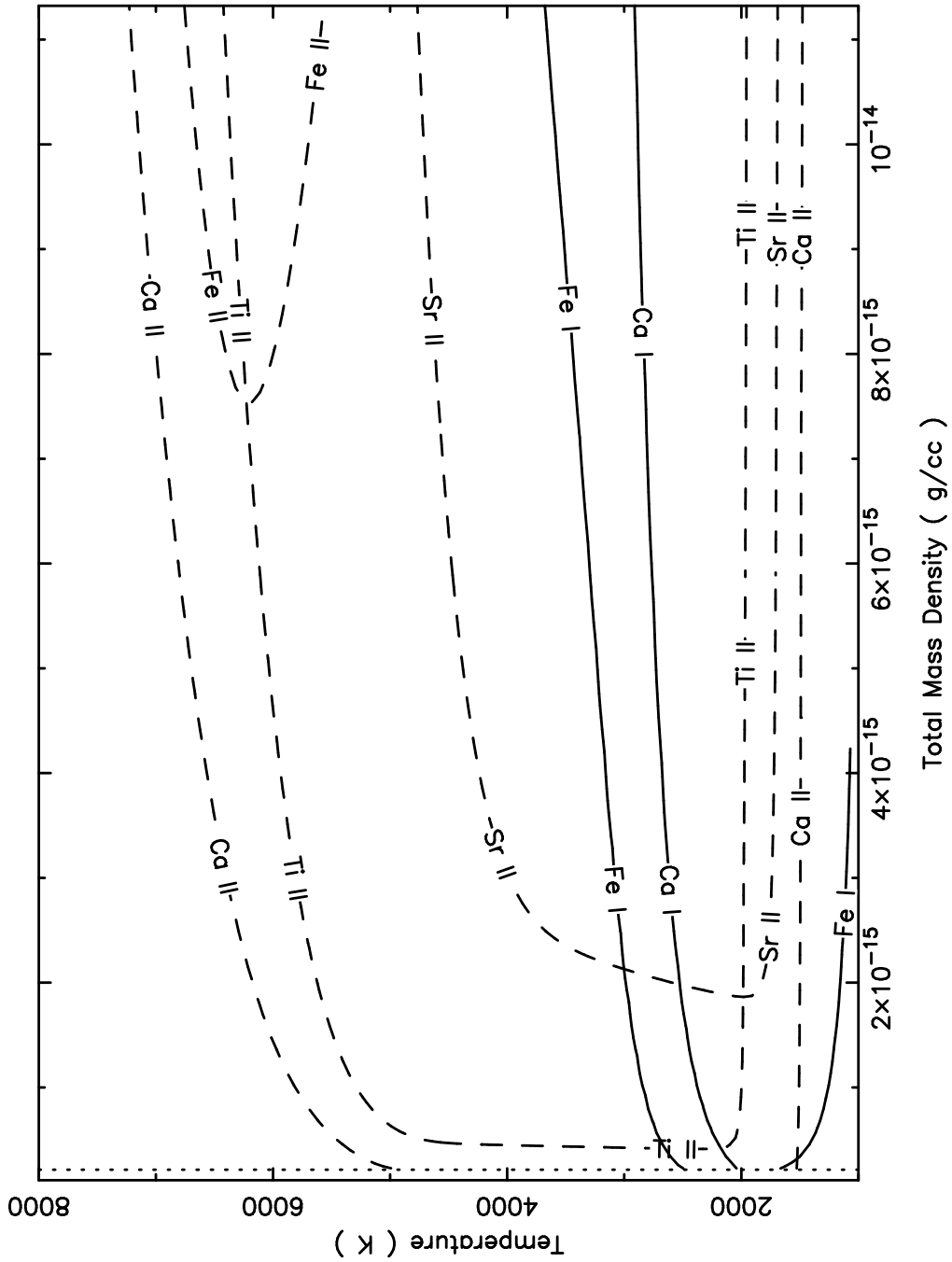


Fig. 12.— Contours of $\tau_{ref} = 1$ of various ions in the C/O-rich composition. Neutral ions are represented with solid contours, and singly ionized ones with dashed contours. The dotted line denotes $\rho_{min}^{C/O} = 2.2 \times 10^{-16}$ g cm⁻³.

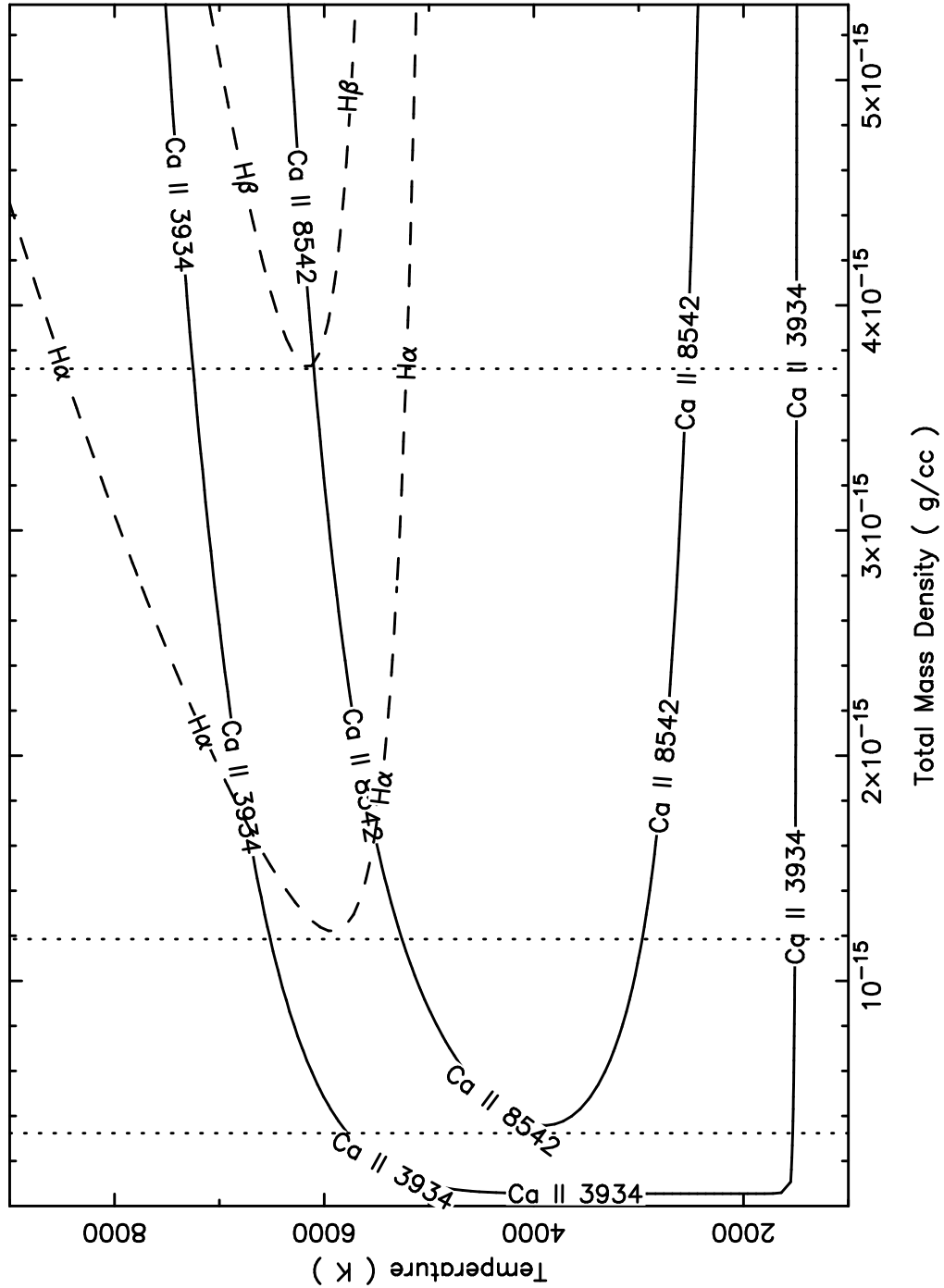


Fig. 13.— Contours of $\tau = 1$ for Ca II $\lambda 3934$ and $\lambda 8542$ H α and H β , assuming the H-rich composition. The dotted lines denote (left to right) $\rho^H = 3.2 \times 10^{-16}$, 1.2×10^{-15} , 3.7×10^{-15} g cm $^{-3}$.

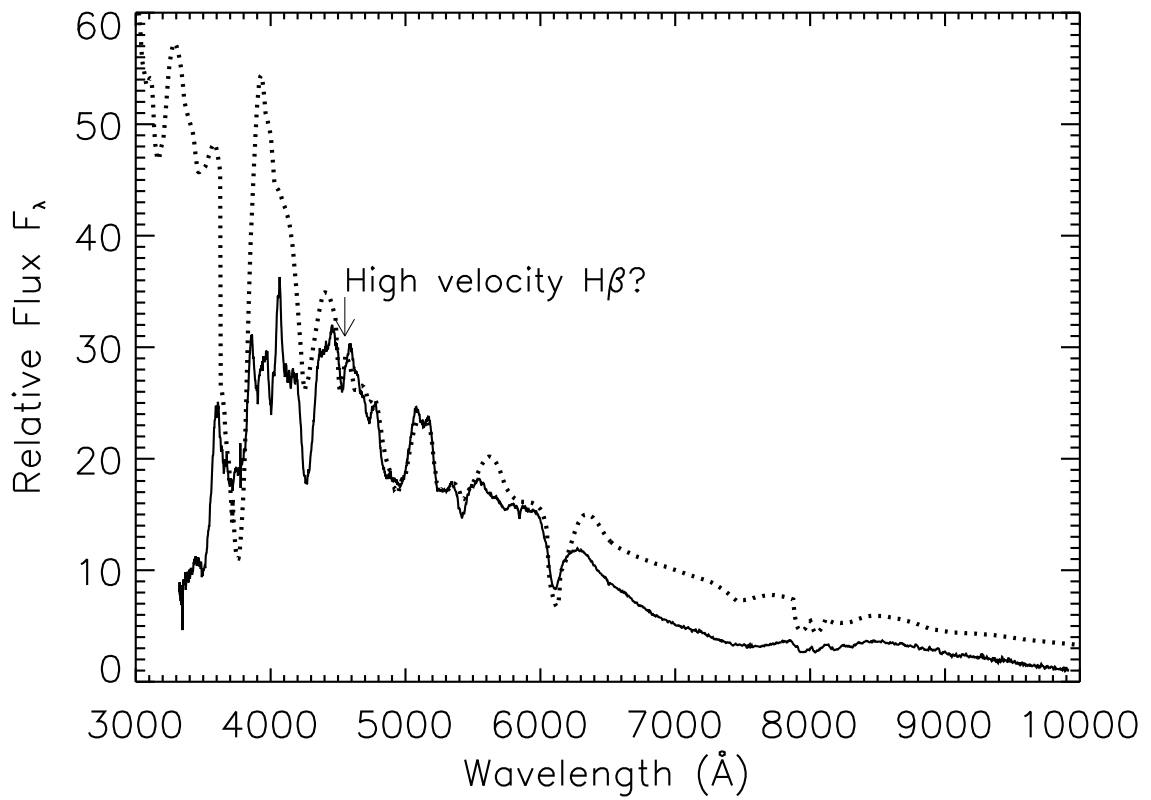


Fig. 14.— Brute fit to SN 2000cx spectrum at two days after maximum, including H optical depth in the HV clump. H α absorption is concealed in the Si II absorption at 6100 Å.

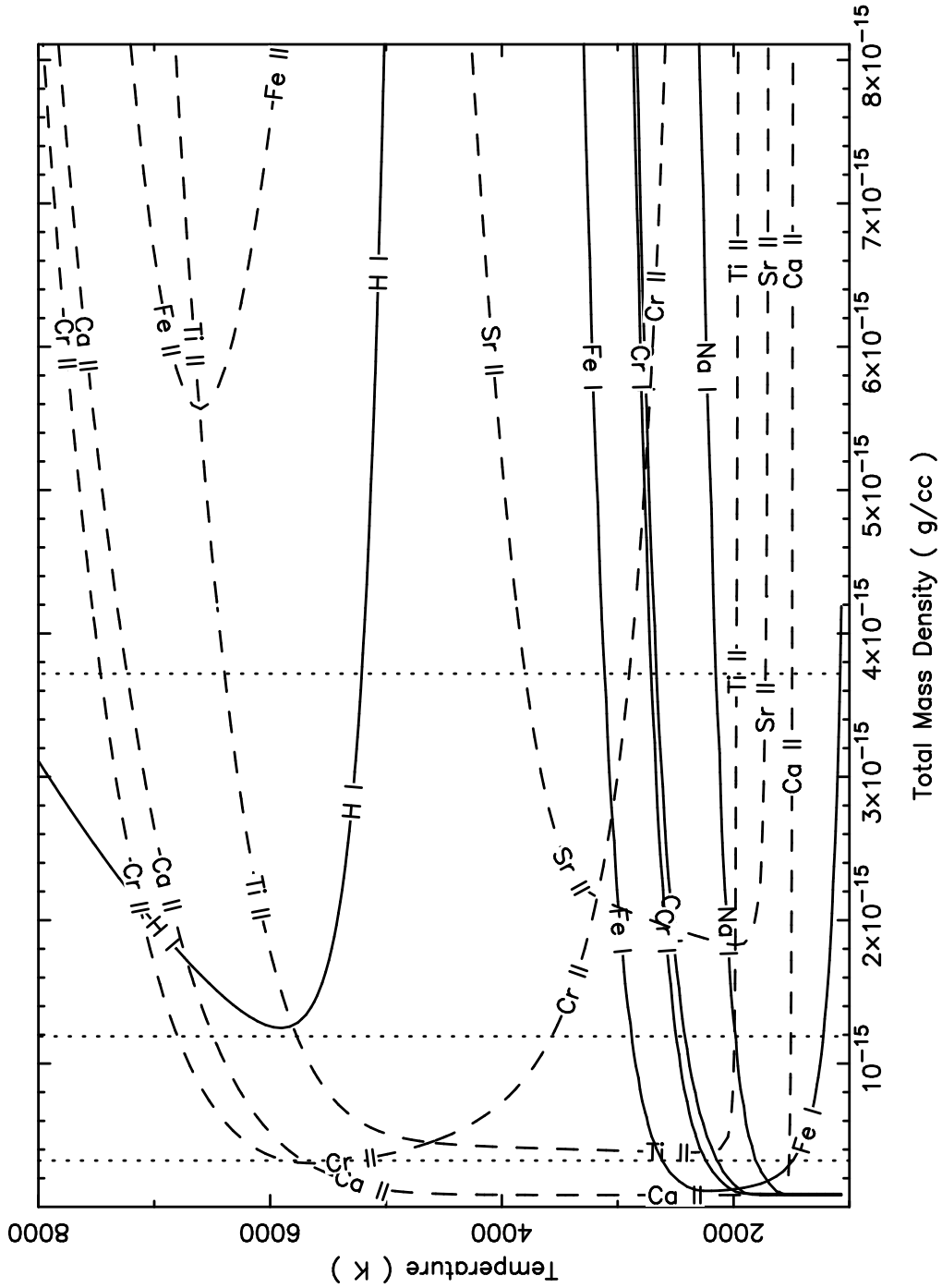


Fig. 15.— Contours of $\tau_{ref} = 1$ of various ions in the H-rich composition. Neutral ions are represented with solid contours, and singly ionized ones with dashed contours. The dotted lines denote (left to right) $\rho^H = 3.2 \times 10^{-16}$, 1.2×10^{-15} , and 3.7×10^{-15} g cm⁻³.